

# Polydispersity enhances the dynamics of Active Brownian particles

Sameer Kumar,<sup>\*</sup> Jay Prakash Singh,<sup>†</sup> Debaprasad Giri,<sup>‡</sup> and Shradha Mishra<sup>§</sup>  
*Department of Physics, Indian Institute of Technology (BHU), Varanasi, U.P. India - 221005*

(Dated: December 23, 2024)

We study the dynamics and the phases of self-propelled disk-shaped particles of different sizes with soft repulsive potential in two dimensions. We observe enhanced dynamics for large size diversity among the particles. Size diversity is defined by the polydispersity index  $\epsilon$ , which is the width of the uniform distribution of the particle's radius. We calculate the steady state diffusion coefficient  $D_{eff}$  and for high self-propulsion speed  $v_0$ , it follows a scaling function  $D_{eff} \sim D_0 \bar{v}_0^\beta f(\epsilon \bar{v}_0^{-\alpha})$ , where  $\alpha$  and  $\beta$  are the two exponents and independent of the self-propulsion speed and the polydispersity index. The phase diagram exhibits a liquid phase with a large number-fluctuations for high self-propulsion speed  $v_0$  and a jammed phase at low  $v_0$  with small number fluctuation. Further, we categorize the phases into solid-jammed and MIPS-liquid for low polydispersity ( $\epsilon$ ) where the particles form periodic clusters. In contrast, we call it liquid-jammed and liquid phase for high  $\epsilon$  where particles form non-periodic clusters. We study the system for three different packing densities of the particles, and the system responds in the same fashion for the polydispersity in the particles' size. Our study can help understand the behavior of cells of various sizes in a tissue, artificial self-driven granular particles, or living organisms of different sizes in a dense environment.

## I. INTRODUCTION

The dynamics of self-propelled particles perpetually moving by converting energy from the environment into mechanical motion and collisions represent a non-equilibrium phenomenon. Such non-equilibrium systems exhibits many interesting properties such as clustering, collective motion [1, 2], anomalous density fluctuations [3], strange rheological behavior [4–6], and activity-dependent phase change [7]. Their size ranges from few microns, e.g., bacteria [8], cells [9], cytoskeletal filament [10], motor proteins [11], etc. to macroscopic systems like fish school, birds flock and animal herds [12], etc.

In 1995 Vicsek and coworkers proposed a swarming model, one of the building blocks to study active matter systems [13]. Colloidal Janus particles [14, 15], which act as an artificial microswimmer due to its asymmetry of surface chemistry, was considered the model system for active matter, often called the active particles. Active particles are generally of two types based on their appearance; elongated rod-like particles are called polar/apolar particles [16], and spherically symmetric particles fall in the category of the active Brownian particles (ABPs). These micron-sized ABPs move in an environment with a low Reynolds number, and hence their dynamics, in general, are overdamped [17–20]. The active Brownian motion appears due to the interplay of self-propulsion and the thermal noise in the system and verified experimentally by studying the collective behavior of colloids and bacteria [17, 18, 20–22].

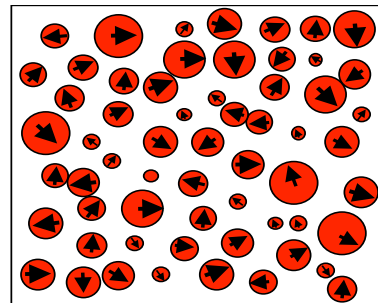


FIG. 1. Schematic diagram of the system for a non-zero polydispersity i.e.  $\epsilon \neq 0$ . Disks in red resembles the active Brownian particles and the arrow shows their local orientation.

Recent studies address the dynamics of ABPs on various environmental backgrounds, e.g., the motion of ABPs on a periodic substrate, channel-based transport of ABPs [23], and dynamics of ABPs in a confined geometry [24], etc. In these studies, apart from the different nature of particle-to-particle interaction (for example, hard or soft repulsive interaction) [25], particles are, in general, considered to be of the same size, i.e., monodisperse. But, there are many cellular systems, bacteria, and colloids that possess size diversity, i.e., all particles do not necessarily have the same radius and can be termed as polydisperse. The polydispersity of the particles' size can lead to many interesting properties in terms of their dynamics.

The self-propelled particle (SPP) model has been described in [26–31] to study such systems. These models are similar to those for inert particulate matter where cells (or bacteria etc.) are represented as disks or spheres that interact with an isotropic soft repulsive potential and electrostatic attraction. Unlike the Brownian particles in a thermal bath, self-propelled

<sup>\*</sup> sameerk.rs.phy16@itbhu.ac.in

<sup>†</sup> jayp.rs.phy16@itbhu.ac.in

<sup>‡</sup> dgiri.app@iitbhu.ac.in

<sup>§</sup> smishra.phy@itbhu.ac.in

particles exhibit persistent random walks. SPP models typically exhibit a glass transition from a diffusive fluid state to an arrested subdiffusive solid that is controlled by (1) the strength of self-propulsion [27, 28, 32] and (2) the packing fraction  $\phi$  [28, 32–35]. Polydispersity also plays a crucial role in these transitions, and it is worth to study the effect of particles' size diversity on the steady-state phase of the system. In, [36] authors have considered self-propelled particles dynamics with some polydispersity, but they do not explicitly explain the effect of particles' size diversity in the system dynamics. In [37], authors have studied the dynamics of tracers with quenched polydispersed obstacles where they have addressed the system for a different amount of polydispersity in the obstacles' size and its effect on the percolation density.

This study addresses the effect of polydispersity in the ABPs system using overdamped Langevin's dynamics to study the particles' dynamics. We model the system with self-propelled disk-like particles on a two-dimensional substrate. The control parameter the diversity in the particles' size is the polydispersity index  $\epsilon$ , which is the width of a uniform probability distribution of particles' radius. System is studied for three different particles density  $\phi = \{0.65, 0.75, 0.85\}$ . Also,  $\phi = 0.85$  is the cut-off packing fraction to remain under the shape rigidity limit [38]. The phase diagram exhibits a liquid phase with a large number-fluctuations for high self-propulsion speed  $v_0$ , which is an inherent property of an active system [3, 39, 40], and a jammed phase at low  $v_0$  with small number fluctuation. Further, we categorize the phases into solid-jammed and MIPS-liquid (i.e. the phase when the system have high diffusivity and shows motility induced phase separation) [35, 41–47] for low polydispersity ( $\epsilon$ ) where the particles form periodic clusters. In contrast, we call it liquid-jammed for high  $\epsilon$  where particles form non-periodic clusters. We also find a scaled plot of the effective diffusion coefficient for different self-propulsion speeds in the liquid phase.

We also compare the system's behavior with its equilibrium counterpart, i.e., the passive Brownian particle. The article is divided in the following manner. In section II, we discuss the model used to study the system; in section III we discuss about the results and finally summarise in section IV.

## II. MODEL AND NUMERICAL DETAILS

We distribute the particles randomly on a two-dimensional substrate. Radius,  $R_i$ , of particles is taken from a uniform distribution  $P(R_i, \epsilon) \in [R_0 - \frac{\epsilon}{2}, R_0 + \frac{\epsilon}{2}]$ , where  $R_0$  is the mean radius and  $\epsilon$  is the width of the distribution and we call it as the polydispersity index (or PDI). We use over-damped Langevin's dynamics to study the system. The equations of motion for particle's dynamics are,

$$\frac{\partial}{\partial t} \mathbf{r}_i(t) = v_0 \hat{\mathbf{e}}_i + \mu \sum_j^N \mathbf{F}_{ij} + \sqrt{2D_T} \eta_i^T(t) \quad (1)$$

$$\frac{\partial}{\partial t} \theta_i(t) = \sqrt{2D_R} \eta_i^R(t) \quad (2)$$

Here,  $\mathbf{r}_i(t)$  is the position of  $i^{th}$  particle at any time  $t$ ,  $v_0$  is the self-propulsion speed and,  $\theta_i(t)$  is the polarity angle which defines  $\hat{\mathbf{e}} = (\cos\theta, \sin\theta)$ . The interaction force between the particles is,  $\mathbf{F}_{ij} = -\nabla U(r_{ij})$ , where  $U(r_{ij})$  is a harmonic potential defined as,

$$U(r_{ij}) = \frac{\kappa}{2} (r_{ij} - \sigma_{ij})^2 \Theta(1 - \frac{r_{ij}}{\sigma_{ij}}) \quad (3)$$

Here,  $\Theta(x) = 1$  for  $x \geq 0$  and;  $\Theta(x) = 0$  for  $x < 0$ .  $r_{ij} = |\mathbf{r}_i - \mathbf{r}_j|$  is the separation between two particles and  $\sigma_{ij} = R_i + R_j$ .  $\kappa$  is the force constant.  $\mu$  is the mobility and is inversely proportional to the friction coefficient such that each particle is driven by a constant force of magnitude equal to  $\frac{v_0}{\mu}$ .  $(\mu\kappa)^{-1}$  is the elastic time scale.  $\eta$  is the random Gaussian white noise with  $\langle \eta(\mathbf{r}, t) \rangle = 0$  and  $\langle \eta(\mathbf{r}, t) \eta(\mathbf{r}', t') \rangle = \delta(\mathbf{r} - \mathbf{r}') \delta(t - t')$ , here  $D_T$  and  $D_R$  are the translational and rotational diffusion coefficient respectively. There is no translational noise i.e  $D_T = 0$  when  $v_0 \neq 0$ , whereas  $D_T \neq 0$  when  $v_0 = 0$  (this is the case when we call the system as *passive*).  $D_R^{-1}$  is the time scale over which the orientation of an active particle changes. Hence,  $l_p = v_0 D_R^{-1}$ , the persistence length or run length, is the typical distance travelled by an active particle before it changes direction. In this model, we fix  $\mu = 1.0$  and  $D_R = 1.0$  throughout the system. Also we study the system for different self propulsion speed i.e.  $v_0 \in (0.1, 1.0)$  and polydispersity  $\epsilon \in (0.0, 0.25)$ . System is studied for three different particles densities  $\phi = \frac{\sum_i^N \pi R_i^2}{L^2} = 0.65, 0.75$  and  $0.85$ , where  $L$  is the size of the system, and  $N$  is the number of particles. We keep the mean radius fixed, i.e.  $R_0 = 0.3$ . The activity  $v_0$  is scaled by by  $R_0 \mu \kappa$  to make it dimensionless i.e.  $\bar{v}_0 = \frac{v_0}{R_0 \mu \kappa}$ , hence  $\bar{v}_0 \in (3.33 \times 10^{-3}, 3 \times 10^{-2})$ . We choose  $\Delta t = 10^{-3}$  in the simulation. Figure 1 shows the schematic diagram for a non-zero polydispersity index  $\epsilon \neq 0$ . Center of the disk shows its position,  $\mathbf{r}$  in the xy-plane and the arrow on it implies the local orientation  $\hat{\mathbf{e}}$ . We can see that for a smaller  $\epsilon (= 0.05)$ , the system looks like mono-dispersed, and for higher value, there is a broad size difference among the particle. Since the particle radius distribution is uniform, smaller and bigger size particles are equal in the number.

## III. RESULTS

Now we study the system properties using Eqs (1) and (2), which governs the time evolution of the system. We

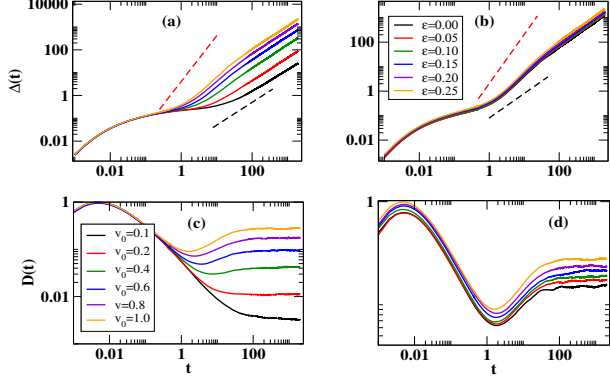


FIG. 2. Plots of mean squared displacement  $\Delta(t)$  vs  $t$  (a,b) and diffusion coefficient  $D(t)$  vs.  $t$  (c,d). (a) and (c) are for different self propulsion speed  $v_0$  and a fixed polydispersity index,  $\epsilon = 0.25$ , whereas as (b) and (d) are for different value of PDI  $\epsilon$  and fixed  $v_0$ . Data is averaged over 15 independent realizations and total time steps in the simulation is  $= 10^7$ .

calculate the different physical quantities and based one that we characterise the system under the different conditions for system variables i.e. packing density  $\phi$ , activity  $v_0$  and polydispersity parameter  $\epsilon$ .

### A. Increase in Diffusivity for finite polydispersity

We characterize the system's properties by calculating the mean squared displacement of the particles for multiple parameter sets. First we calculate the mean squared displacement (MSD)  $\Delta(t)$  defined as  $\Delta(t) = \langle \frac{1}{N} \sum_i^N [\mathbf{r}_i(t) - \mathbf{r}_i(0)]^2 \rangle$ , where  $\langle \dots \rangle$  means the average over many initial configurations. Fig. 2, shows the plot of MSD and diffusion coefficients,  $D(t) = \frac{\Delta(t)}{4t}$ , for different activity i.e. self-propulsion speed  $v_0$  and polydispersity index  $\epsilon$  for packing density  $\phi = 0.85$ . In fig. 2(a) we plot the MSD for different  $v_0$  and fixed PDI  $\epsilon = 0.25$ . We perceive that early time dynamics ( $t < 0.01$ ) are ballistic, followed by a plateau, and then start diffusing latter ( $t > 100$ ). The late-time dynamics ( $t > 100$ ) is a persistent random walk where the MSD grows linearly with time. The plateaus region appears for a longer time for lower self-propulsion speed and decreases with an increase in  $v_0$ ;—the plateaus region surfaces due to the over-damped dynamics in the system. Further, when we increase the value of  $v_0$ ,  $\Delta(t)$  shift upward in the positive y-axis i.e. increase in diffusion coefficient  $D(t)$  (2(c)). Next, in figure 2(b), we see a similar trend a fixed activity and different PDI  $\epsilon$ , i.e., as we increase PDI, MSD shift upwards. This leads to the diffusion coefficient increase, shown in  $D(t)$  vs.  $t$  plot in fig. 2(d).

We do similar calculation for other parameters and plot the steady state diffusion coefficient in fig. 3 for different

packing fractions. We define effective diffusion coefficient<sup>3</sup>  $D_{eff}$  in steady state ( $t > 100$ ) as  $D_{eff} = \lim_{t \rightarrow \infty} D(t)$  for different self propulsion speed  $v_0$  and polydispersity index  $\epsilon$ . Fig. 3(a-c) shows the variation of  $D_{eff}$  for different activity and for different packing fractions,  $\phi$ . We found that the diffusivity vs. self propulsion speed have a slope  $\beta \simeq 2.0$  for all  $\phi$ 's = 0.65, 0.75 and 0.85. Further, in fig. 3(d-f), we plot  $D_{eff}$  vs  $\epsilon$ , also we fit the data points with the expression for diffusion coefficient given by  $D_{eff}(\epsilon, v_0) = v_0^\beta D_0(\phi)[1 + \exp(\frac{\epsilon}{\epsilon_c})]$ , where  $D_0$  is the diffusivity for monodisperse system ( $\epsilon = 0$ ) and depends only on the packing density of the system. It shows that as we increase the size diversity among the ABPs, diffusivity of the system increases and the change is high for high activity in the system (which is explained in more detail in the next paragraph). In fig. 4(a), we plot  $\epsilon_c$  vs  $v_0$  for different packing fractions,  $\phi$  and observe a non-monotonic change in  $\epsilon_c$  on varying  $v_0$ . On increasing  $v_0$  first it increases and reaches a maximum and then decreases for larger  $v_0$ . Hence we find that  $\epsilon_c \sim v_0^\alpha$ , where  $\alpha \simeq 0.18$  for  $v_0 \leq 0.3$  and  $\alpha \simeq -0.20$  for  $v_0 \geq 0.4$ . Using this information we find a scaled plot of  $D_{eff} \times v_0^{-\beta}$  vs  $\epsilon \times v_0^\alpha$  for different  $\phi$ , fig. 4(b-d). We find good scaling collapse of data for all  $\phi$ 's and different  $v_0 \geq 0.4$ . Hence, for  $v_0 \geq 0.4$ , diffusivity of the system can be give by the scaling function  $D_{eff} \sim D_0 v_0^\beta f(\epsilon v_0^{-\alpha})$ , where  $\alpha$  and  $\beta$  are the scaling constants and independent of the system parameters  $v_0, \epsilon$  and  $\phi$ ; whereas,  $D_0$  only depends on  $\phi$  and have the values 0.265, 0.15 and 0.072 for  $\phi = 0.65, 0.75$  and  $0.85$  respectively.

### B. Mobility order parameter

Now we explain the enhanced dynamics due to the polydispersity. First, we analyze the effect of activity on the system dynamics, and then we study the impact of the polydispersity. In a self-driven system, particles do not stay static for a long time; instead, they keep moving throughout the system. The crowding of the environment makes the particles to collide among themselves during motion. Hence, their instantaneous speed is not the same, but some move faster and some slower. We defined *rattlers* in the system based on the crowding in the neighbourhood of a particle. A particle with two or less immediate neighbour(s) is called 'rattler' and hence it is more mobile until it loses the tag. In a d-dimension, a particle can be a rattler if it has less than  $d + 1$  neighbour(s). In fig. 6(a-b), we show the snapshots from the simulation from two different polydispersity, where the particles that are rattlers are in blue, whereas those are non-rattler are in red. We calculate the mobility order parameter (MOP)  $\psi(t)$  defined as  $\psi(t) = \frac{N_r(t)}{N}$ , where  $N$  is the number of particle in the system and  $N_r$  is the number of rattlers. Also,  $\psi \in (0, 1)$ , if  $\psi = 1$  means that all the particles in the system are rattlers and vice versa. This tells us that the higher the value of the MOP, the system will

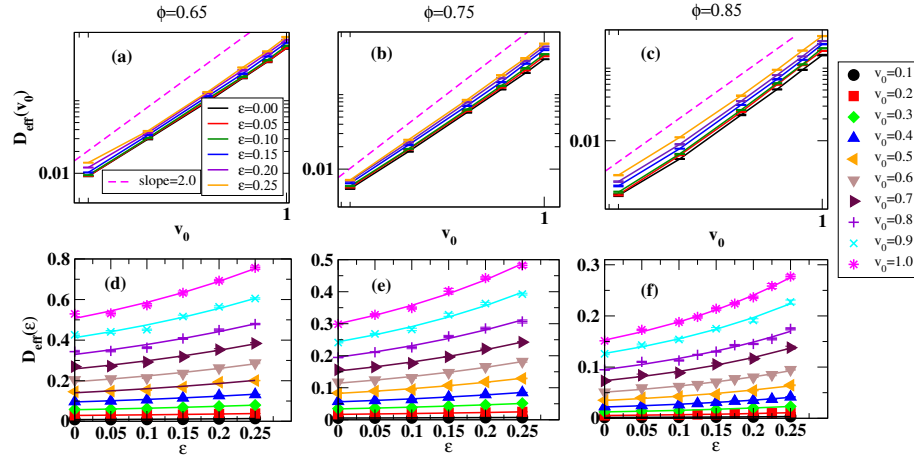


FIG. 3.  $D_{eff}$  vs.  $v_0$  for different values of  $\phi$  (a-c).  $D_{eff}$  vs.  $\epsilon$  for different values of  $\phi$  (d-f), symbols are from the simulation and the solid lines are the fit to the data points. Fitting function is  $D_{eff} = v_0^\beta D_0 [1 + \exp(\frac{\epsilon}{\epsilon_c})]$ ,  $\beta$  is the slope of  $D_{eff}$  vs.  $v_0$  plot and have values equal to 1.82, 1.84 and 2.0 for  $\phi = 0.65, 0.75$  and 0.85 respectively.

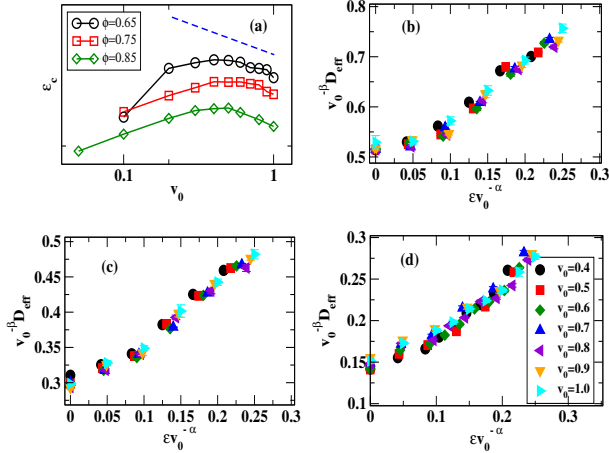


FIG. 4. (a) Critical PDI ( $\epsilon_c$ ) vs  $v_0$ , where  $\epsilon_c$  is obtained by fitting the data from the simulation by  $D_{eff} = v_0^\beta D_0 [1 + \exp(\frac{\epsilon}{\epsilon_c})]$ , dashed line have the slope =  $-0.2$ . Scaled plot for  $D_{eff}$  vs.  $\epsilon$  for the packing fraction  $\phi = 0.65$  (b),  $\phi = 0.75$  (c) and  $\phi = 0.85$  (d). Here y-axis is scaled as  $D_{eff} \rightarrow \frac{D_{eff}}{v_0^\beta}$  and the x-axis is scaled as  $\epsilon \rightarrow \frac{\epsilon}{v_0^\alpha}$ , here  $\alpha$  is the slope of  $\epsilon_c$  vs  $v_0$  and is equal to 0.18 for  $v_0 \leq 0.3$  and  $\alpha = -0.20$  for  $v_0 \geq 0.4$  for all  $\phi$ . Also,  $\beta$  is the slope of  $D_{eff}$  vs.  $v_0$  plot and have values equal to 1.82, 1.84 and 2.0 for  $\phi = 0.65, 0.75$  and 0.85 respectively.

be more dynamical. Further, we define  $\psi_{bs} = \frac{N_{rb}(t)}{N_{rs}(t)}$ , where  $N_{rb}$  is the number of those rattlers whose radius i.e.  $R_i > R_0$  and  $N_{rs}$  are the number of rattlers whose radius i.e.  $R_i \leq R_0$ .

In fig. 5(a-b) we plot the probability distribution functions  $P(\psi)$  vs.  $\psi$ ; and in 5(c-d) we plot  $P(\psi_{bs})$  vs.  $\psi_{bs}$  for  $\phi = 0.85$  for different system parameters. In fig. 5(a), peak of  $P(\psi)$  shift towards smaller values of  $\psi$  which suggest that the number of rattlers in the system decreases with an increase in  $v_0$  and hence MSD should also decrease, but we see opposite to this. This is

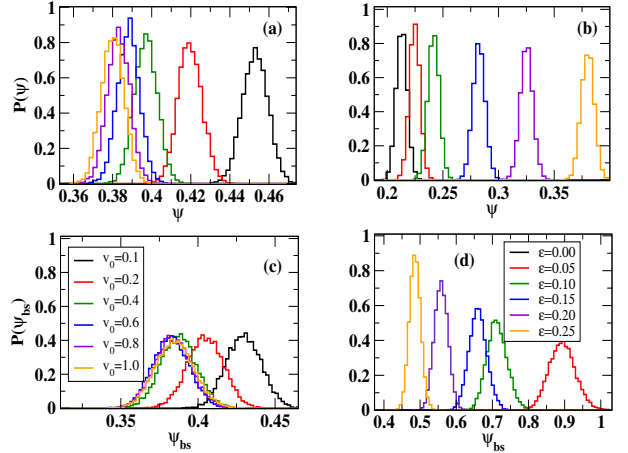


FIG. 5. Plots of  $P(\psi)$  vs  $\psi$  and  $P(\psi_{bs})$  vs  $\psi_{bs}$ , where  $\psi$  and  $\psi_{bs}$  are the dynamic order parameters. (a) and (c) are for different self propulsion speed  $v_0$  and a fixed PDI,  $\epsilon = 0.25$ , whereas as (b) and (d) are for different value of  $\epsilon$  and fixed  $v_0$ .  $P(\psi)$  is the probability distribution function calculated from the time series plot of  $\psi(t)$  vs.  $t$  plot (not shown here). Data is averaged over 15 independent realizations and total time steps in the simulation is  $= 10^7$ .

because for a non-zero PDI, peak of  $P(\psi_{bs})$  also shifted towards smaller values (see fig. 5(c)) which implies that  $N_{rs}$  is higher than the  $N_{rb}$ , and we know that smaller particles have higher *peclet number*  $P_e$  (since  $P_e \propto \frac{v_0}{R_i}$ ) and hence for a fixed  $v_0$  the contribution of smaller particles (when  $R_i \leq R_0$ ) to the MSD is higher than that for bigger ones (i.e.  $R_i > R_0$ ). Eventually, we see an increase in the MSD, hence, higher  $D_{eff}$  for a higher value of self-propulsion speed.

Similarly, we can explain the increase in  $D_{eff}$  if we increase  $\epsilon$ . Fig. 5(b) shows that the peak of  $P(\psi)$  shifts towards higher values and that of  $P(\psi_{bs})$  towards left. This implies that with an increase in PDI, rattlers are increasing, but small rattlers increase more, which have

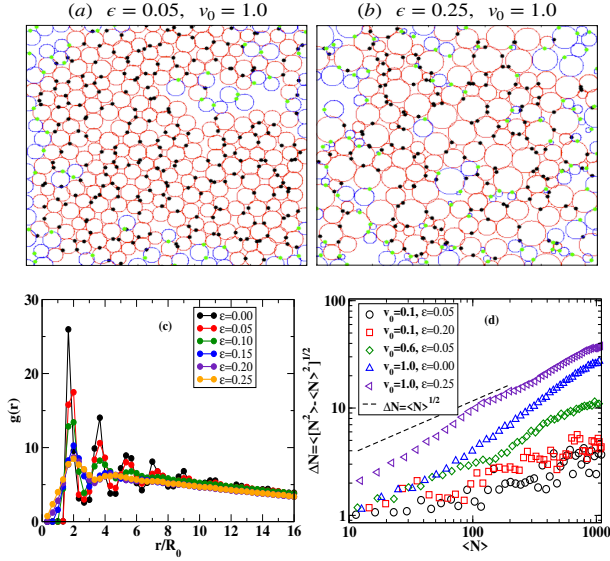


FIG. 6. (a) and (b) are the snapshots at equal time for  $\epsilon = 0.05$  and  $\epsilon = 0.25$  respectively and fixed  $v_0 = 1.0$ . Rattlers are represented by blue circles whereas non-rattlers are in red. Black and green dots at the surface of the circles show the direction of motion. (c) is the plots of radial distribution function  $g(r)$  for different value of PDI,  $\epsilon$  and fixed velocity. (d) Number Fluctuation for different set of  $(\epsilon, v_0)$  for  $\phi = 0.85$ .

much higher motility than bigger ones. Hence the  $D_{eff}$  increases with an increase in PDI.

### C. Phase diagram:

In the previous paragraph, we discussed the effect of the polydispersity on the system dynamics where we have calculated the steady-state diffusion coefficient of the system. We study different phases in the system based on the structures of the particle cluster and the number fluctuation. First, to understand the structure of particle cluster we calculate the radial distribution function  $g(r)$ .  $g(r)$  is a measure of the probability of finding a particle at  $\mathbf{r}_2$  given a particle at  $\mathbf{r}_1$ ;  $r = |\mathbf{r}_1 - \mathbf{r}_2|$ . In two dimensions  $\langle n \rangle g(r) d^2\mathbf{r}$  gives the number of particles in  $d^2\mathbf{r}$ , where  $\langle n \rangle$  is the mean number of particle in unit area. In fig. 6(a-b), we show the snapshots for two different values of PDI ( $\epsilon$ ). We plot  $g(r)$  vs. normalise radial distance  $\frac{r}{R_0}$  in fig. 6(c), and see that with an increase in PDI, not only the height of the peak of  $g(r)$  decreases, but also the distribution loses its periodicity since the number of peaks reduces. This means the structure of the distribution of the particles in the system shifted to the less ordered liquid-like structure (for higher  $\epsilon$ ) from the more ordered solid one (for  $\epsilon = 0$ ). Also, if  $g(r)$  have at least three peaks in  $g(r)$  vs.  $r/R_0$  plot, this represents a near to hexagonal closed pack (HCP) structure (fig. 6a), and we call it as a solid-like structure

TABLE I. List of value of  $\epsilon$  and  $D_{eff}$  and the corresponding phase.  $m$  in the number of peaks in the  $g(r)$  plot,  $\gamma$  is the exponent in  $\Delta N \sim N^\gamma$ .

| $\epsilon$ | $D_{eff}$               | $m$      | $\gamma$   | Phase                  |
|------------|-------------------------|----------|------------|------------------------|
| $\leq 0.1$ | $D_{eff} \leq 0.05$     | $\geq 3$ | $< 0.5$    | <i>solid – jammed</i>  |
| $> 0.1$    | $D_{eff} \leq 0.05$     | $< 3$    | $< 0.5$    | <i>liquid – jammed</i> |
| $\leq 0.1$ | $D_{eff} > 0.05$        | $\geq 3$ | $\geq 0.5$ | <i>MIPS – liquid</i>   |
| $> 0.1$    | $0.05 < D_{eff} < 0.25$ | $< 3$    | $\geq 0.5$ | <i>Liquid</i>          |
| $> 0.1$    | $D_{eff} \geq 0.25$     | $< 3$    | $\geq 0.5$ | <i>liquid</i>          |

whereas when it has less than three peaks, we call it as a liquid-like structure (far away from HCP) (fig. 6b). Next, we calculate the number fluctuation, defined as  $\Delta N = \sqrt{\langle N^2 \rangle - \langle N \rangle^2}$ , where  $\Delta N$  is the standard deviation is the number of particles in different size subcells.  $\Delta N \sim \langle N \rangle^\gamma$ , it has been found that  $\gamma > 0.5$  for the ABP undergoing MIPS [35, 41–47].

It suggests large number fluctuations in the active system undergoing dynamical phase separation. Whereas in the corresponding equilibrium system  $\gamma \leq 0.5$ . On the other hand, in systems with the frozen or jammed state,  $\gamma < 0.5$  [36]. Hence  $\Delta N$  is a measure of fluctuations in the number of particles in different subcells. In fig. 6(d), we show the plot for the number fluctuation for a chosen sets of  $(v_0, \epsilon)$ , and observe that for small value of  $v_0$  ( $= 0.1$  in the plot) system shows small number fluctuation and giant number fluctuation for higher  $v_0$  ( $v_0 = 0.6$  and  $1.0$  in the plot).

In table I, we list the observed values of  $D_{eff}$ ,  $m$  (which is the number of peaks in  $g(r)$  plot) and  $\gamma$ , and based on this we define the different phases of the system for the system parameters i.e.  $(v_0, \epsilon)$ . Now, we explicitly discuss the different phases in the system and show the phase diagram in fig. 7.

*solid-jammed and liquid-jammed phase:* We call the system to be in the solid-jammed state when the  $g(r)$  vs  $\frac{r}{R_0}$  have at least three peaks ( $m \geq 3$ ) and  $D_{eff} \leq 0.05$ , whereas system is said to be in the liquid jammed phase when  $D_{eff} \leq 0.05$  but  $g(r)$  vs  $\frac{r}{R_0}$  plot have less than three peaks ( $m < 3$ ), which implies that the structure of the particles distribution in the system is far away from the periodic structure. Further, to confirm the state of the system for the given parameters, we found that the in number fluctuation plot,  $\Delta N \sim N^\gamma$ ,  $\gamma \leq 0.5$ , this implies that the number fluctuations in different size subcells are small and hence, particles are jammed. We observe that for  $v_0 \leq 0.4$  and all PDI, the system is in jammed phase for a different amount of packing fractions,  $\phi$ .

*Liquid Phase:* We call the system to be in the liquid phase when  $D_{eff} \geq 0.25$ , also, the number of peaks in the radial distribution function is essentially less than three i.e.  $m < 3$ . The number fluctuation exponent  $\gamma > 0.5$  i.e. the system shows a giant number fluctuation. We observe that for  $v_0 \geq 0.4$  and  $\epsilon \geq 0.15$ , system is in liquid phase for different amount of packing fractions,  $\phi$ .

*MIPS-liquid Phase:* In this case,  $m \geq 3$ ,  $D_{eff} > 0.05$



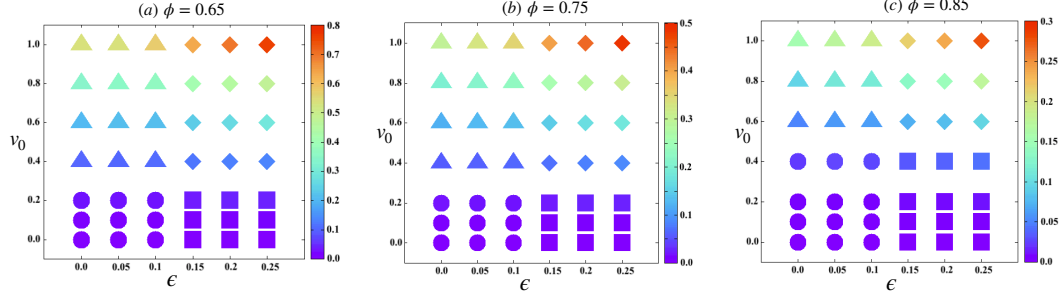


FIG. 7. Phase diagram for  $\phi = 0.65$  (a),  $\phi = 0.75$  (b) and  $\phi = 0.85$  (c): filled circles, squares, diamonds and triangles represents the solid-jammed phase, liquid-jammed phase, MIPS phase and liquid phase respectively.

and the number fluctuation exponent  $\gamma \geq 0.5$ . We call it the MIPS-liquid phase since  $m \geq 3$  as the particles form periodic clusters (similar to HCP). The previous studies found that for polar disk-like particles of the same sizes, phase separate due to the system's inherent motility, and termed as motility induced phase separation (MIPS) [35, 41–47]. We observe that for  $v_0 \geq 0.4$  and  $\epsilon \leq 0.1$ , system is in MIPS-Liquid phase for different amount of packing fractions,  $\phi$ .

In fig. 7, we show the phase diagram for different packing fractions. Different symbols imply the type of the phase for the given parameter set, and the color bar shows the value of  $D_{eff}$  for the same. We also observe that for  $\phi = 0.65$  and  $0.75$ , system show jammed phase for  $v_0 \leq 0.3$  whereas it is jammed for  $v_0 \leq 0.4$  for  $\phi = 0.85$ . This shift is due to the particles' high packing density, which makes the system highly crowded; hence, it needs higher activity to be in the liquid phase.

#### D. Comparison to the passive system

We calculate the mean squared displacement  $\Delta(t)$  and  $D_{eff}(t)$  for a system of polydispersed passive Brownian particles, where we chose  $v_0 = 0$  and  $D_T \neq 0$ . Also, we take the value of  $D_T$  such that the thermal noise in the system generate an equivalent force among the particle as it is a non-zero  $v_0$ , and compare the results. We keep  $v_0$  to be fixed and equal to 1.0 and the thermal noise comparable to  $v_0 = 1.0$  is calculated using the definition  $\frac{v_0^2}{D_T D_R} \equiv \frac{v_0}{D_R R_0}$ , where  $D_T, D_R$  are the translational and rotational diffusion coefficients respectively,  $v_0$  is the self-propulsion speed and  $R_0$  is the mean radius. From this we find the equivalent noise in the system  $D_T = 0.3$  for  $v_0 = 1.0$ . Fig. 8 (a) shows the  $\Delta(t)$  vs  $t$  plot for ABPs and its passive equivalent. Fig. 8(b) shows the  $D_{eff}(\epsilon)$  vs.  $\epsilon$  plot, which suggests that the effective diffusivity in the active case is very high than that of the passive case. Fig. (c-d). We also plot the  $D(t)$  vs.  $t$  separately for small and big particles, fig. 8(c-d). We can see the difference in the diffusion coefficient for both and find that the effect of polydispersity is relatively less in the passive case than that of the active case. This tells us

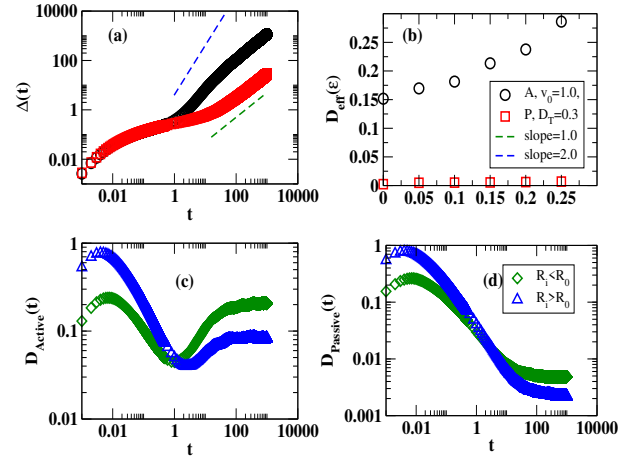


FIG. 8. Comparative plots for physical quantities for ABPs and its passive counter part. We keep  $v_0$  to be fixed and equal to 1.0. (a)  $\Delta(t)$  vs  $t$  plot, (b)  $D_{eff}(\epsilon)$  vs.  $\epsilon$  plot, (c)  $D_{small}(t)$  vs  $t$  plot, (d)  $D_{big}(t)$  vs.  $t$  plot, where  $D_{small}$  and  $D_{big}$  stand for diffusion coefficient of small particles (with  $R_i \leq R_0$ ) and big particles (with  $R_i > R_0$ ).

that polydispersity's response is much larger for the active Brownian particles than their passive counterpart. Besides quantitative differences in the physical observables, qualitatively, the passive system's response for polydispersity is similar to what has been observed in the active case.

#### IV. DISCUSSION

We study the dynamics and the phases of self-propelled disk-shaped particles of different sizes with soft repulsive potential in two dimensions. The system is analyzed mainly for two variables, the *activity* in the system, which is controlled by the self-propulsion speed of the particles  $v_0$ , and the diversity in particles' size, which is defined by the polydispersity index,  $\epsilon$ , which is the width of the uniform distribution of the particle's radius. We study the system for low Reynolds' number and hence, use over-damped Langevin's dynamics to study the particles' motion. We observe enhanced dynamics for

large size diversity among the particles. We calculate the steady-state diffusion coefficient  $D_{eff}$  and for high self-propulsion speed  $v_0$ , it follows a scaling relation  $D_{eff} \sim D_0 \bar{v}_0^\beta f(\epsilon \bar{v}_0^{-\alpha})$ ,  $\alpha = -0.2$  and  $\beta \simeq 2.0$ , are the scaling exponents. We also calculate the mobility order parameter to understand the enhanced dynamics for a non-zero polydispersity. We find a phase diagram in the plane of  $(\epsilon, v_0)$  and it exhibits a liquid phase with a large number-fluctuations for high self-propulsion speed  $v_0$  and a jammed phase at low  $v_0$  with small number fluctuation. Further, we categorize the phases into solid-jammed and MIPS-liquid for low polydispersity ( $\epsilon$ ) where the particles form periodic clusters. In contrast, we call it liquid-jammed for high  $\epsilon$  where particles form non-periodic clusters. We study the system for three different packing densities of the particles and observe almost the same trend in the properties. Further, we do the same study for an equivalent passive case and find that the effect of polydispersity is rela-

tively less in the passive case than that of the active case.

Our analysis can help understand the behavior of cells of various sizes in a tissue, artificial self-driven granular particles, or living organisms of different sizes in a dense environment.

*Acknowledgement :* SM and SK, thanks DST-SERB India, ECR/2017/000659 for the financial support. The support and the resources provided by PARAM Shivay Facility under the National Supercomputing Mission, Government of India at the Indian Institute of Technology, Varanasi are gratefully acknowledged. Computing facility at Indian Institute of Technology(BHU), Varanasi is gratefully acknowledged.

## V. REFERENCES

- 
- [1] A. Gopinath, M. F. Hagan, M. C. Marchetti, and A. Baskaran, Phys. Rev. B 85, 061903 (2012).
  - [2] F. Peruani, A. Deutsch, and M. Bar, Phys. Rev. E 74, 030904 (2006).
  - [3] S. Ramaswamy, R. A. Simha, and J. Toner, Europhys. Lett. 62, 196 (2003).
  - [4] L. Giomi, T. B. Liverpool, and M. C. Marchetti, Phys. Rev. E 81, 051908 (2010).
  - [5] D. Saintillan, Phys. Rev. E 81, 056307 (2010).
  - [6] M. E. Cates, S. M. Fielding, D. Marenduzzo, E. Orlandini, and J. M. Yeomans, Phys. Rev. Lett. 101, 068102 (2008).
  - [7] T. Shen and P. G. Wolynes, Proc. Natl. Acad. Sci. U.S.A. 101, 8547 (2004).
  - [8] Dombrowski, C., L. Cisneros, S. Chatkaew, R.E. Goldstein, and O. Kessler, 2004, Phys. Rev. Lett. 93, 098103.
  - [9] J. Kemkemer, R., D. Kling, D. Kaufmann, and H. Gruler, 2000, Eur. Phys. J. E 1, 215.
  - [10] Surrey, T., F. J. Nedelec, S. Leibler, and E. Karsenti, 2001, Science 292, 1167.
  - [11] Bendix, P. M., G. H. Koenderink, D. Cuvelier, Koeleman, W. M. Briehera, C. M. Fielda, L. Z. Dogic, B. N. Mahadevan, and D. A. Weitz, 2008, Biophys. J. 94, 3126.
  - [12] T. Vicsek and A. Zafeiris, Phys. Rep. 517, 71 (2012).
  - [13] T. Vicsek, A. Czirok, E. Ben-Jacob, I. Cohen, and O. Shochet, "Novel type of phase transition in a system of self-driven particles," Phys. Rev. Lett. 75, 1226 (1995).
  - [14] H.-R. Jiang, N. Yoshinaga, and M. Sano, Phys. Rev. Lett. 105, 268302 (2010).
  - [15] G. Volpe, I. Buttinoni, D. Vogt, H.-J. Kummerer, and C. Bechinger, Soft Matter 7, 8810 (2011).
  - [16] M. C. Marchetti et. al. Hydrodynamics of soft active matter, Review of Modern Physics, 85, 2013.
  - [17] J. R. Howse, R. A. Jones, A. J. Ryan, T. Gough, R. Vafabakhsh, and R. Golestanian, "Self-motile colloidal particles: from directed propulsion to random walk," Phys. Rev. Lett. 99, (2007).
  - [18] B. tenHagen, S. van Teeffelen, and H. Lowen, "Non-gaussian behaviour of a self-propelled particle on a substrate," Condens. Matter Phys. 12, 725–738 (2009).
  - [19] B. ten Hagen, S. van Teeffelen, and H. Lowen, "Brownian motion of a self-propelled particle," J. Phys.: Condens. Matter 23, 194119 (2011).
  - [20] F. Kummel, B. ten Hagen, R. Wittkowski, I. Buttinoni, R. Eichhorn, G. Volpe, H. Lowen, and C. Bechinger, Phys. Rev. Lett. 110, 198302 (2013).
  - [21] C. Kurzthaler, C. Devailly, J. Arlt, T. Franosch, W. C. Poon, V. A. Martinez, and A. T. Brown, Phys. Rev. Lett. 121, 078001 (2018).
  - [22] C. Bechinger, R. Di Leonardo, H. Lowen, C. Reichhardt, G. Volpe, and G. Volpe, "Active particles in complex and crowded environments," Rev. Mod. Phys. 88, 045006 (2016).
  - [23] S. Pattanayak, R. Das, M. Kumar, S. Mishra, The European Physical Journal E 42 (5), 62, 2019.
  - [24] Suchismita Das, Sounok Ghosh, and Raghunath Chelakkot, Phys. Rev. E 102, 2020.
  - [25] P. Dolai, A. Simha, S. Mishra, Phase separation in binary mixtures of active and passive particles, Soft Matter, 2018.
  - [26] J. M. Belmonte, G. L. Thomas, L. G. Brunnet, R. M. C. de Almeida, and H. Chaté, Self-Propelled Particle Model for Cell-Sorting Phenomena, Phys. Rev. Lett. 100, 248702 (2008).
  - [27] S. Garcia, E. Hannezo, J. Elgeti, J.-F. Joanny, P. Silberzan, and N. S. Gov, Proc. Natl. Acad. Sci. U.S.A. 112, 15314 (2015).
  - [28] S. Henkes, Y. Fily, and M. C. Marchetti, Active Jamming: Self-Propelled Soft Particles at High Density, Phys. Rev. E 84, 040301 (2011).
  - [29] N. Sepulveda, L. Petitjean, O. Cochet, E. Grasland-Mongrain, P. Silberzan, and V. Hakim, Collective Cell Motion in an Epithelial Sheet Can be Quantitatively Described by a Stochastic Interacting Particle Model, PLoS Comput. Biol. 9, e1002944 (2013).
  - [30] S. S. Soumya, A. Gupta, A. Cugno, L. Deseri, K. Dayal, D. Das, S. Sen, and M.M. Inamdar, Coherent Motion of Monolayer Sheets under Confinement and Its Patho-

- logical Implications, PLoS Comput. Biol. 11, e1004670 (2015).
- [31] B. Szabo, G. J. Szöllösi, B. Gönci, Zs. Jurányi, D. Selmeczi, and T. Vicsek, Phase Transition in the Collective Migration of Tissue Cells: Experiment and Model, Phys. Rev. E 74, 061908 (2006).
  - [32] R. Ni, M. A. C. Stuart, and M. Dijkstra, Pushing the Glass Transition towards Random Close Packing Using Self-Propelled Hard Spheres, Nat. Commun. 4, 2704 (2013).
  - [33] L. Berthier, Nonequilibrium Glassy Dynamics of Self-Propelled Hard Disks, Phys. Rev. Lett. 112, 220602 (2014).
  - [34] Y. Fily, S. Henkes, and M. C. Marchetti, Freezing and Phase Separation of Self-Propelled Disks, Soft Matter 10, 2132 (2014).
  - [35] Y. Fily and M. C. Marchetti, Athermal Phase Separation of Self-Propelled Particles with No Alignment, Phys. Rev. Lett. 108, 235702 (2012).
  - [36] Silke Henkes, Yaouen Fily, and M. Cristina Marchetti, Active jamming: Self-propelled soft particles at high density, Phys. Rev. E 84, 040301(R) 2011.
  - [37] Arun Yethiraj et. al. , Effect of Polydispersity on Diffusion in Random Obstacle Matrices, Phys. Rev. Lett., vol 109, 2012.
  - [38] F. Bolton and D. Weaire, Rigidity Loss Transition in a Disordered 2D Froth, Phys. Rev. Lett., vol 65, 1990.
  - [39] J. Toner, Y. Tu, and S. Ramaswamy, Ann. Phys. (N.Y.) 318, 170 (2005).
  - [40] J. Toner and Y. Tu, Phys. Rev. Lett. 75, 4326 (1995).
  - [41] G. S. Redner, M. F. Hagan and A. Baskaran, Phys. Rev. Lett., 2013, 110, 055701.
  - [42] J. Stenhammar, A. Tiribocchi, R. J. Allen, D. Marenduzzo and M. E. Cates, Phys. Rev. Lett., 2013, 111, 145702.
  - [43] J. Tailleur and M. E. Cates, Phys. Rev. Lett., 2008, 100, 218103.
  - [44] G. Gonnella, A. Lamura and A. Suma, Int. J. Mod. Phys. C, 2014, 25, 1441004.
  - [45] A. Suma, D. Marenduzzo, G. Gonnella and E. Orlandini, Europhys. Lett., 2014, 108, 56004.
  - [46] D. Levis and L. Berthier, Phys. Rev. E, 2014, 89, 062301.
  - [47] R. Wittkowski, A. Tiribocchi, J. Stenhammar, R. Allen, D. Marenduzzo and M. E. Cates, Nat. Comm., 2014, 5, 4351.